Synthesis of highly conductive, uniformly silver coated carbon nanofibers by electroless deposition

AUTHOR NAMES:

*Xavier Cauchy[†], Jolanta-Ewa Klemberg-Sapieha[‡], Daniel Therriault[†]**

AUTHOR ADDRESS:

[†] Department of Mechanical Engineering, École Polytechnique de Montréal. 2900 boul. Édouard-Montpetit, Montréal, QC, Canada, H3T 1J4

[‡]Department of Engineering Physics, École Polytechnique de Montréal, 2900 boul. Édouard-Montpetit, Montréal, QC, Canada, H3T 1J4.

*Corresponding Author : daniel.therriault@polymtl.ca

KEYWORDS

Electroless deposition, conductive fillers, carbon nanofibers, silver coating, Tollens' reagent, nanoparticles decoration

ABSTRACT

Noble metal coated carbon-based nanoparticles when used as electrically conductive fillers have the potential to provide excellent conductivity without the high weight and cost normally

associated with metals such as silver and gold. To this effect, many attempts were made to deposit uniform layers of metals on core nanoparticles with an emphasis on silver for its high conductivity. The results so far were disheartening with the metal morphology being better described as a decoration than a coating with small effects on the electrical conductivity of the bulk particles. We tackled in this work the specific problem of electroless deposition of silver on carbon nanofibers (CNFs) with the investigation of every step of the process. We performed X-ray photoelectron spectroscopy (XPS), transmission and scanning electron microscopy (TEM, SEM), Zeta potential and electrical conductivity measurements to identify a repeatable, reliable set of parameters allowing for a uniform and fully connected silver deposition on the surface of the CNFs. The bulk particles' specific electrical conductivity (conductivity per unit mass) undergoes a more than ten-fold increase during the deposition, reaching 2500 $S \cdot cm^2/g$, which indicates that the added metal mass participates efficiently to the conduction network. The particles keep their high aspect ratio through the process, which enables a percolated conduction network at very low volume loadings in a composite. No by-products are produced during the reaction so the particles do not have to be sorted or purified, can be used as produced and the reaction time is ~15 minutes. The particles might be an interesting replacement to conventional fillers in isotropic conductive adhesives, as a conductive network is obtained at a much lower loading. They might also serve as electrically conductive fillers in composites where a high conductivity is needed, such as lightning strike protection systems, or as high surface area silver electrodes.

1. INTRODUCTION

Electrically conductive nanoparticles have attracted considerable attention from researchers because of their ability to impart electrical transport properties to otherwise insulating polymers. Applications such as isotropic conductive adhesives (ICAs) for heat sensitive electronics [1] or lightning strike protection for composite aircraft skins [2] require very high conductivities for efficiency and safety, respectively. Carbon nanotubes (CNTs) were heavily investigated as electrically conductive fillers [3-7] because of the potentially very high transport capabilities of individual particles [8]. Moreover, these particles were shown to allow electrical transport in polymers at very low concentrations because of their high aspect ratio [4, 6]. However, the electrical performance of CNT-loaded composites always lagged behind expectations with maximum conductivities in the range 10^{-3}-10^{-1} S/m [4, 9-11], far lower than the typical 10^{7} S/m value for high conductivity metals. The explanation for this disappointing performance lies in a strong tunneling resistance between individual particles [5] and in high contact resistance depending on the configuration of the adjacent particles [12]. There is also an important disparity between the conductivity values of CNT-filled polymers [6] since dispersion state, nanotube type and surface treatment have considerable impact on the end result [4, 13]. For these reasons, the fillers of choice for isotropic conductive adhesives remain metallic. Silver particles are the norm since silver has the highest conductivity of all metals. Moreover, silver nanostructures have been shown to be able to sinter at low temperature [14], under microwave irradiation [15], chemically at room temperature [16] and with infrared irradiation [17]. Silver however suffers from two principal drawbacks: it is expensive and, at 10.49 g/cm^3, it is heavy. These two drawbacks can be diminished by lowering the silver content in the composite material. Increasing the aspect ratio of fillers is a proven strategy in order to obtain lower percolation thresholds and thus a higher conductivity at a lower loading [18]. However, major obstacles remain to the scalability of silver

nanowires production. Among these, a time consuming purification process, loss of silver metal inherent to the polyol method, long synthesis times and low production rates are often cited [19-21].Our strategy is then to circumvent these shortcomings by using high aspect ratio carbonaceous particles as templates for electroless deposition of silver to obtain high aspect ratio hybrid particles with low metal to metal inter-particle contact resistance and thus provide an alternative path for high performance electrically conductive nanofillers.

Electroless deposition is a technique used extensively in the last century to produce mirrors [22-23], but was since set aside in favor of processes more efficient for flat geometries. It has however been revisited lately for applications in nanotechnology, where small complicated geometries cannot be coated with vapor deposition processes [24]. Electroless deposition was successfully used to metallize complicated microstructures [24-25] and to fabricate surface plasmon resonance sensors [26] and surface-enhanced Raman scattering substrates [27-28]. Deposition on carbonaceous substrates has been attempted with varying success. The conductivity of graphite-filled ICAs was shown to increase by up to two orders of magnitude with electroless silver deposition [29-30] and a uniform coating was obtained on carbon spheres [31-32], but the deposition on nano-sized particles proved to be more challenging. The process applied to carbon nanotubes resulted in mere decoration [33-34], a discontinuous coating [35-38] or loss of aspect ratio [39-40]. Arai *et al.* did show convincingly that pure nickel and Ni-B alloy electroless deposition on vapor-grown nanofibers could yield an excellent coating uniformity [41-42]. The same group attempted silver electroless deposition with silver iodide and dimethylaminoborane as a reducing agent. The method was less successful as the coating continuity was not achieved [43].

We herein show that electroless deposition of silver metal on carbon nanofibers (CNFs) can result in a smooth silver coating with preservation of the particles' high aspect ratio. We provide

detailed analysis of every step of the process, namely functionalization, sensitization and deposition through the use of X-ray photoelectron spectroscopy (XPS), transmission electron microscopy (TEM), scanning electron microscopy (SEM) and electrical conductivity measurements, among others. We provide a window of working parameters for each step with insight into possible underlying mechanisms. We finally show that the process results in uniformly silver coated carbon nanofibers with improved bulk electrical conductivity.

2. EXPERIMENTAL SECTION

2.1. FUNCTIONALIZATION

CNFs (PR-25-XT-HHT Pyrograf® Products Inc.) were acquired from Sigma Aldrich. The nanofibers have a nominal diameter of 100 nm and a nominal length between 50 and 200 μm. Functionalization was carried out by immersing 1g of CNFs in 70 mL of a mixture of HNO_3 (Anachemia ACS 68-70%) and H_2SO_4 (Anachemia ACS 95-98%) in the volume ratio of 1:3 and sonicating it for 3 hours in an ultrasonication bath (42 kHz Cole-Parmer 08891-11). Alternatively, CNFs were functionalized by refluxing in the same acid mixture in a round bottom flask with magnetic stirring. The flask was immersed in a silicon oil bath heated to various temperatures and the reaction was performed for 1 and 3 h. The functionalized particles were filtered out using 0.4 μm pore diameter polycarbonate membranes and a vacuum filtration apparatus. Particles were rinsed with deionized water until a neutral pH was reached and were then stored in deionized water.

2.2. SENSITIZATION

Stannous chloride dihydrate ($SnCl_2 \cdot 2H_2O$, 98%) from manufacturer Alfa Aesar was acquired from VWR. All solutions were obtained by first dissolving the $SnCl_2$ in deionized water to obtain a 10 g/L concentration, and adding various amounts of HCl to dissolve the precipitate (more details will be discussed in Results and discussion Section). Functionalized CNFs were filtered out from the deionized water and dispersed in the acidic $SnCl_2$ solution by mechanically disrupting aggregates with a stirring rod in 10 ml of solution. 30 ml of solution was added and the mixture was sonicated for 2 minutes. Aggregates were then decanted and the procedure was repeated until a nanofiber concentration of 625 mg/L was reached. The dispersion was then placed in a sealed glass bottle and sonicated for 45 minutes, followed by a 90 min dwell and another 45 min sonication with temperature kept below 45 °C, as confirmed through monitoring with a thermocouple. Particles were filtered out of the solution by vacuum filtration and redispersed in deionized water. The rinsing operation was repeated 5 times and the filtrate was tested for Cl^- ions by adding aqueous silver nitrate ($AgNO_3$). If Cl^- ions are present in solution, silver chloride (AgCl) precipitates and the solution turns cloudy. Sensitized CNFs were stored in 18 MΩ pure water at a concentration of 100 mg CNFs for 350 mL H_2O.

2.3. TOLLENS' REAGENT

$AgNO_3$ (ACS reagent, Alfa Aesar) acquired from VWR was dissolved in 60 mL of 18 MΩ pure water for a 0.5 M concentration. Under magnetic stirring, 1 mL of a 6×10^{-2} M KOH solution was added to the solution. At this point the solution exhibits a cloudy yellow color. Ammonium hydroxide (Alfa Aesar, 28% NH_3) was then added dropwise. The solution turned dark brown before it gradually cleared up and became transparent again. Just enough ammonia was added to make the solution transparent, which amounts to ~4-5 mL, depending on the residual NH_3 content in the reagent.

2.4. REDUCING SOLUTION

For the investigation of the effect of Tollens' reagent volume, a reducer master batch was prepared by adding 6 mL of denatured ethanol to 36 g of a 20% dextrose solution. 70 g of a sensitized CNF dispersion with 0.029% CNF content by weight was added to the reducer master batch. The resulting solution was divided equally into 8 glass vials.

For the investigation of the effect of dextrose concentration, 8.75 g of the same sensitized 0.029% CNF dispersion masterbatch was added to each of 8 glass vials. After adding 3.6 mL of pure water, dextrose was added in quantities varying from 35.5 mg to 4.544 g, doubling the concentration from sample to sample and keeping the water mass the same as in the investigation of Tollens' reagent volume. 750 µL of ethanol was then added to each sample.

2.5. REACTION

The Tollens' reagent was added to the glass vials containing the sensitized CNFs and the reducing solution. The vials were closed airtight and were agitated for 15 minutes for the reaction to proceed. The solution was then poured in 40 mL of deionized water and rinsed twice with 80 mL of deionized water by vacuum filtration. The resulting nanoparticles, in layers evenly deposited on a polycarbonate membrane, were dried overnight under vacuum and weighed.

2.6. CHARACTERIZATION

Electrical conductivity was measured using a 4 point probe (Jandel 100µm tip, 1 mm spacing, linear array) hooked to a current source (Keithley 220) and multimeter (Hewlett Packard 34401A). Three sets of voltage vs. current measurements were obtained on different zones of the sample and a two parameter linear fit was performed to determine the conductivity value. The

error on conductivity values corresponds to the standard deviation of the conductivity value for the different data sets.

SEM images were obtained using a JEOL JSM7600F field emission scanning electron microscope in secondary electron imaging mode. The acceleration tension was set at 10.0 kV with a working distance of approximately 8 mm. TEM images were obtained on a JEOL JEM-2100F microscope equipped with a field emission electron gun. Acceleration voltage was 200 kV.

XPS was performed using a VG scientific ESCALAB 3MKII apparatus with the Mg Kα ray as the X-ray source. The sampling depth was 50-100 Å. The background subtraction was performed with the Shirley method and atomic sensitivity factors derived by Wagner.

Zeta potential was measured using a Malvern Instruments Zetasizer Nano ZSP analyzer. The sensitized CNF solution was diluted to 20 times its volume before analyzing. The Malvern universal dip cell with a glass cuvette was used. Zeta potential was calculated using the Smoluchowski method.

3. RESULTS AND DISCUSSION

3.1. STARTING MATERIAL & FUNCTIONALISATION

As-received CNFs are described by the manufacturer as having a stacked-cup core with a graphitized chemical vapor deposited carbon overcoat. Figure 1-a shows a schematic of the

nanofiber structure: the graphitic planes organize in a conical shape, which stacks in the axial direction. Graphitization of the vapor-deposited carbon at 3000 °C causes the atoms to organize in concentric graphitic planes, similar to the structure of multiwall carbon nanotubes. Figure 1-b is a TEM image of the as-received particles that confirms the structure of a typical nanofiber. However, roughly 10% of the fibers observed exhibited the structure depicted in Figure 1-c and d, which is commonly known as the *bamboo shaped* structure. Figure 1-e shows a high-resolution XPS spectrum obtained for the as-received product. The analysis showed a very clean 100% carbon signal. The inset shows a magnification of the $C1_S$ asymmetrical peak typical of highly graphitic carbon. The component at 286.4 eV represents 88.7 at. % and is attributable to carbon bonding in the sp^2 hybridization state. The remaining 11.3 at. % are found at 291.3 eV, typical of bonding-antibonding transitions in π orbitals accompanying sp^2 carbon. The absence of sp^3 carbon is indicative of a highly graphitic surface.

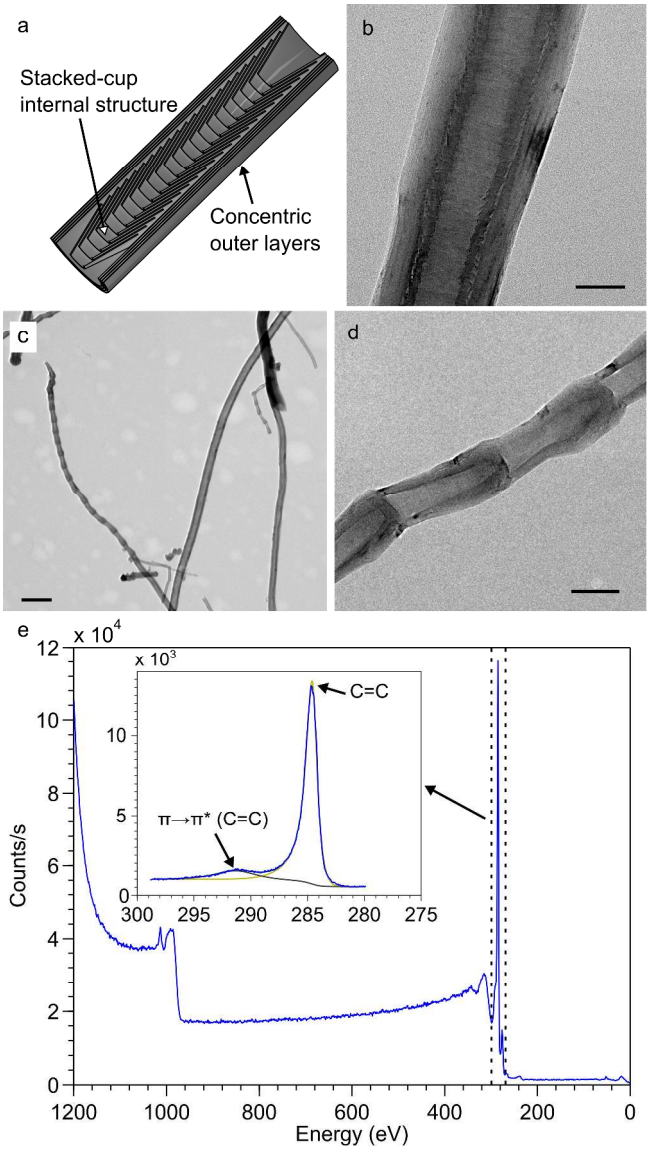

Figure 1. As-received CNFs characterization. a) Schematics of the CNF graphitic planes structure. b) TEM image showing the concentric and stacked cup regions of a typical CNF (scale bar 50 nm). c) TEM image showing the high aspect ratio of the CNFs both bamboo shaped and concentric-stacked cup type (scale bar 1 μm). d) A close-up of a bamboo shaped CNF. The graphitic planes configuration is clearly visible (scale bar 100 nm). e) XPS survey of pristine CNFs. Only the carbon peak is visible. The inset shows a high resolution spectrum of the carbon C 1s peak. It shows only graphitic carbon, with the corresponding bonding-anti bonding peak

The CNFs were acid functionalized to ensure a clean surface and enhance wetting for the subsequent sensitization step. A 3:1 vol. H_2SO_4:HNO_3 mixture is a proven acid mixture for attachment of oxygen-containing groups on the surface of CNTs and CNFs [44]. We investigated the effect of different times and temperatures on the surface composition of functionalized CNFs with XPS. The results are summarized in Table 1. Other than the extent of the functionalization, the conservation of the structural integrity of the nanoparticles is of prime importance since high aspect ratio conductive particles are sought at the final step of the process. It was shown that functionalization in this particular mixture of acids leads to a loss of material, and therefore a strong degradation of the particles' structure starting at a mixture temperature of 70 °C, and that the yield is as low as 30% for a temperature of 100 °C [44]. Data in Table 1 shows that the surface oxygen content of nanoparticles treated at 60 °C is considerably lower than for those treated at 75 and 90 °C. However, a comparison of the increase in oxygen content in particles treated for 1 and 3 hours shows that it doubles for particles treated at 60 °C while it stays nearly constant for those at 90 °C. This suggests that the acid treatment will give equivalent results at low temperature if performed for longer times while preserving the CNF aspect ratio.

Table 1. Oxygen at. % on CNF surface for different treatment conditions.

Method	Refluxing					Ultrasonic agitation
Time (h)	1			3		3
Temperature (°C)	60	75	95	60	90	< 45
oxygen atomic %	5.2	10.2	14.2	10.6	15.1	11.7

We also investigated acid treatment coupled with ultrasonic agitation for low temperature functionalization. The same mixture was immersed in the ultrasonic bath for 3 hours before filtration. During the treatment, the water bath temperature rose from 23 °C to 45 °C because of the dissipated ultrasonic energy. The resulting oxygen content was 11.7%, which is higher than for a 3 h treatment at 60 °C without ultrasonication. Since the goal is to avoid the degradation of nanoparticles and low yield associated with an acid mixture temperature over 70 °C, we needed to verify to what extent the nanoparticle structure was affected by sonication. Figure 2-a shows a TEM image of CNFs after ultrasonically assisted functionalization. The image confirms that the high 100+ aspect ratio is conserved through the low temperature ultrasonically assisted treatment. Figure 2-b shows the typical damage found after functionalization: a faint band is visible on the particle boundary that is attributable to lifted graphitic planes, although roughly half the particles did not display any noticeable damage. Overall, the structure of the nanoparticles was preserved. Figure 2-c and d present the high resolution XPS spectra from the

carbon and oxygen peaks of functionalized nanofibers. The peak at 289.3 eV in the C1s spectrum is attributed to O–C=O bonds with 3.9 at.% and the peaks at 287.8 and 286.6 eV are attributed to C=O and C–O bonds at 2.8 and 2.7 at.%, respectively. The presence of these bonds on the surface of functionalized CNFs is consistent with groups usually found on acid-functionalized carbon [45], with a slight prevalence of carboxylic acids. The O1s peak shows a total oxygen at.% of 12.7. Convoluted in the O1s peak is detected 2.7 at.% oxygen pertaining to adsorbed water that wasn't found on pristine nanofibers, further confirming the increased hydrophilicity of acid functionalized carbon nanofibers [44-45]. To assess the extent of the increase in hydrophilicity, pristine and acid functionalized CNFs buckypapers were subjected to the sessile drop method for angle of contact measurements. Figure 3 shows an example of such measurements. On average, the functionalized CNFs showed a decrease of 15.3° in contact angle. Although modest, this increase in hydrophilicity is desired for enhanced wetting during the tin sensitization treatment.

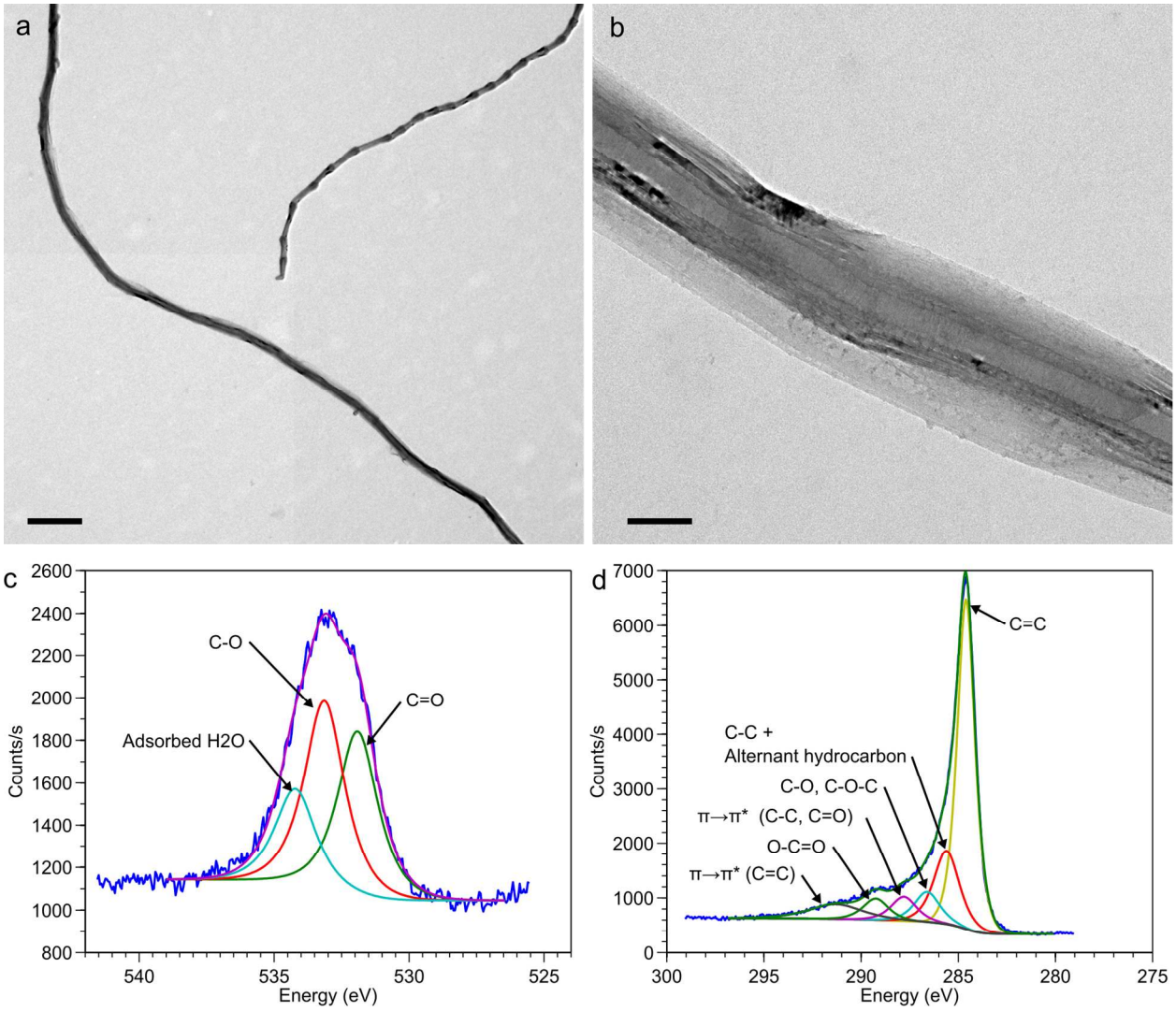

Figure 2. Functionalized CNFs characterization. a) TEM image showing that the aspect ratio (~100) is preserved through functionalization (scale bar, 1µm). b) TEM showing lifted graphitic planes at the nanofiber surface. This is the type of damage that can be found on ultrasonically assisted acid functionalization of CNFs (scale bar, 100 nm). c) XPS high resolution spectrum of the O1s peak created by functionalization. The bonds are consistent with carboxylic functional groups. d) High resolution spectrum of the C1s peak. The importance of O–C=O relative to C–O and C=O bonds show a slight prevalence of carboxylic acid groups. Many new bonds are formed compared to pristine CNFs (Figure 1-e).

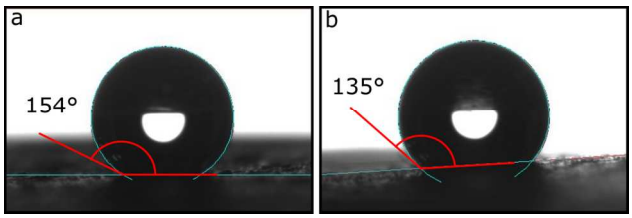

Figure 3. Contact angle measurements of water on CNF buckypapers. a) pristine CNF buckypaper. b) Acid functionalized buckypaper. The average decrease of 15° indicate a modest increase in hydrophilicity after functionalization

SENSITIZATION

The silver deposition process is initiated by reduction of Ag^{-} by Sn^{2+} on the surface to be coated [32]. The distribution of tin seeds on the CNFs during sensitization is therefore crucial to the quality of the subsequently deposited silver film. We performed sensitization by immersing the functionalized nanofibers in a $SnCl_2$ solution with the addition of HCl and exposing it to ultrasonic energy. The HCl concentration was shown to have an important influence over Sn(II) oxidation to Sn(IV) [46], activator seed density and contact angle [47]. All these parameters are thought to affect the deposited metal film quality. We therefore chose to vary HCl concentration in the $SnCl_2$ solution and investigate its effect on the dispersion stability and on the zeta potential. HCl was added in 6 concentration values logarithmically varying from 20 to 640 mM. Figure 4 shows the sedimentation behavior of sensitized nanofibers with HCl concentration values increasing from left to right. Figure 4-a shows particles in the sensitizing solution, after the whole sonication cycle was completed. Functionalized CNFs will disperse spontaneously in the $SnCl_2$ solution up to an HCl concentration of 160 mM. Samples 5 and 6 in Figure 4 have concentrations of 320 and 640 mM HCl respectively. The nanofibers in these samples could not be dispersed even with sonication times up to 2 hours. Figure 4-b shows the sensitized nanofibers

4 hours after 5 cycles of rinsing with 40 mL deionized water and moderate vial agitation to redisperse the filtered particles. Sample 6 in Figure 4-b shows more sedimentation than all the other samples. This particular sample also showed numerous visible aggregates which were absent from the other dispersions. The samples were then sonicated for 10 minutes and left untouched for sedimentation assessment. Figure 4-c shows the dispersions after settling for 90 hours. The stability of the dispersions increased gradually from 20 to 320 mM, and decreased for the highest concentration. Poor wetting of nanofibers was also noticeable in the latter case where some particles remained preferentially on the air-water interface and adhered to the vial walls.

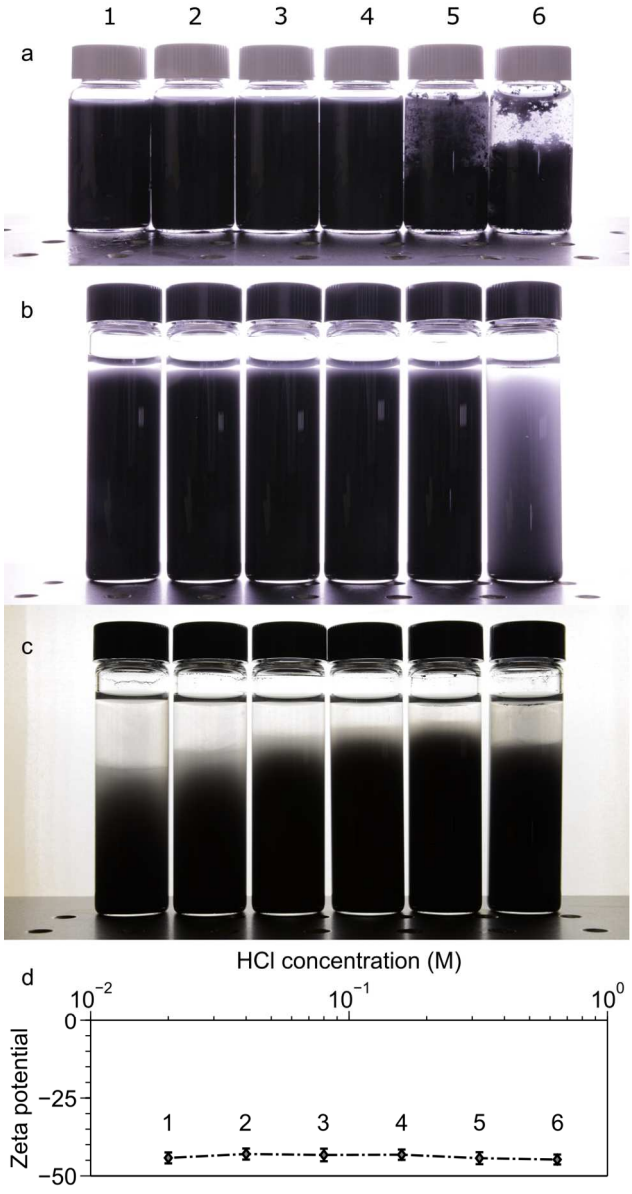

Figure 4. Sedimentation behavior and zeta potential for sensitized CNFs. HCL concentration doubles in each sample, from 20 mM (#1) to 640 mM (#6). a) Particles in the $SnCl_2$ solution at the end of the sonication process. CNFs do not disperse in the 320 and 640 mM solutions. b) Rinsed particles in deionized water. No ultrasonic power was applied for dispersion. The sample with 640 mM HCl does not disperse spontaneously. c) Same as b), with 10 min. ultrasonic agitation and 90 hours sedimentation. The settling time increases with concentration until 320

mM (sample 5). d) Zeta potential of the the dispersions in c) diluted to 10 times their volume. No significant variation was measured.

The sedimentation speed of the particles is influenced mainly by particle size and density [48]. Incidentally, flocculation will accelerate the settling of the dispersion by forming larger aggregates which are less subjected to the dispersing effects of Brownian motion. Flocculation occurs when the zeta potential barrier is not high enough to shield particles from their neighbor's attractive van der Walls forces. To assess whether zeta potential differences were responsible for different settling times, we measured the potential on 0.5 mL of each dispersion diluted to 10 mL. The measured values are presented in Figure 4 d). Surprisingly, the zeta potential values were fairly constant over the range of concentrations studied. Another interesting fact lies in the negative value of the potential for neutral pH aqueous media. It was shown that sensitization reduces silver mainly by oxidation of Sn(II) species to Sn(IV) [49]. The simplest scheme for sensitization would then correspond to adsorption of Sn^{2+} ions on the surface of CNFs along with an adsorbed H_2O layer. Upon drying, Sn^{2+} ions would be exposed to oxygen and allowed to be oxidized to Sn^{4+}, with probable formation of SnO_2, which would explain the necessity to keep the surface wet, as Sn(IV) species were shown to be unable to initiate electroless deposition [49]. However, this scheme would result in a positive Zeta potential, which was not observed here. A more detailed scheme was edified by Cohen and West [50] which involves colloid formation around the naturally present Sn^{4+} species by polymerization of $Sn(OH)_4 \cdot nH_2O$. These colloids will in turn bind Sn^{2+} ions for a ratio close to 1 Sn^{2+} ion per 2 Sn^{4+} ions. The authors show convincingly in another publication [51] that it is these colloids that are adsorbed on the surface to be sensitized. The measured Zeta potential would then correspond to the colloids' potential.

Further research could confirm whether the zeta potential of Sn colloids alone correspond to our observations on CNFs.

Further observations support the adsorbed colloids theory. Generally speaking, as particles are left to settle the zeta potential barrier is broken and van der Walls forces dominate, making the sediments hard to redisperse. The strategy for preventing sediments formation is the addition of thickeners such as hydroxyethylcellulose [48]. Here, the settled particles are very easily dispersed, supporting the idea that the tin colloids act as a thickener, preventing the particles from coming close enough together for the van der Walls forces to dominate. The difference in settling time must then be attributable to particle size. Since the starting particles underwent identical preparation steps, the additional mass must be added by the tin sensitization. It was shown [50] that the hydrolysis leading to $Sn(OH)_4$ could be inhibited by the presence of Cl^- ions in excess of 500 mM. Without this Sn(IV) complex, the colloids formation cannot occur. In support of this finding, samples 5 and 6, respectively approaching and crossing the 500 mM threshold, show a dramatic decrease in dispersibility in Figure 4-a. Moreover, in subsequent water dispersions, sample 6 does not recover and marks a rupture in the sedimentation behavior trend. This confirms that the sensitization does indeed enter a different regime when Cl^- ions in the sensitization bath cross a concentration threshold around ~500 mM. It was also noted that the solution with the lowest HCl concentration clogged the membrane pores during the filtration process, with dramatically decreased flow through the membrane. This observation is consistent with the model where the colloids are sensitive to pH. High HCl concentration dissolves the outer layers, resulting in smaller colloids [50]. The lowest HCl concentration value therefore allows for larger colloids which block water flow through the filter pores. It is interesting to underline here that the sensitization treatment allows for a remarkable stability of carbon nanoparticle

dispersions. This finding alone may facilitate developments based on CNFs or CNTs, since efficient dispersion is a major concern in the field of nanocomposites manufacturing.

To the best of our knowledge, no direct high resolution images of sensitization deposits were available in the literature prior to our work. Figure 5 shows high resolution TEM images of sensitized particles at 60 (Figure 5-a) and 160 (Figure 5-b) mM HCl concentrations. Compared to the functionalized CNF in Figure 2-a and b, we notice that the sensitization yields small spherical particles of 2-3 nm diameter on the surface of the nanofibers. A rough estimate based on Figure 5-b shows that the density of tin particles is around 1.5×10^5 particles/μm^2 which is one order of magnitude higher than the value obtained by Feldstein et al. on formvar [52]. Measurement of inter planar spacing on individual particles yielded a value of 3.4 Å, consistent with the [110] direction of the SnO_2 lattice [53-54]. The lattice dimension is further confirmed by noticing very similar inter planar spacing in tin particle planes and in the underlying graphitic structures. Figure 5-a displays bare patches without any tin particles. It is unclear why these patches are more common for the 60 mM HCl concentration sample. However, since particles settle faster at both low and high HCl concentrations and since the 160 mM sample shows better uniformity than that at 60 mM, we chose to proceed with a 160 mM HCl concentration for the investigation of the silvering process parameters.

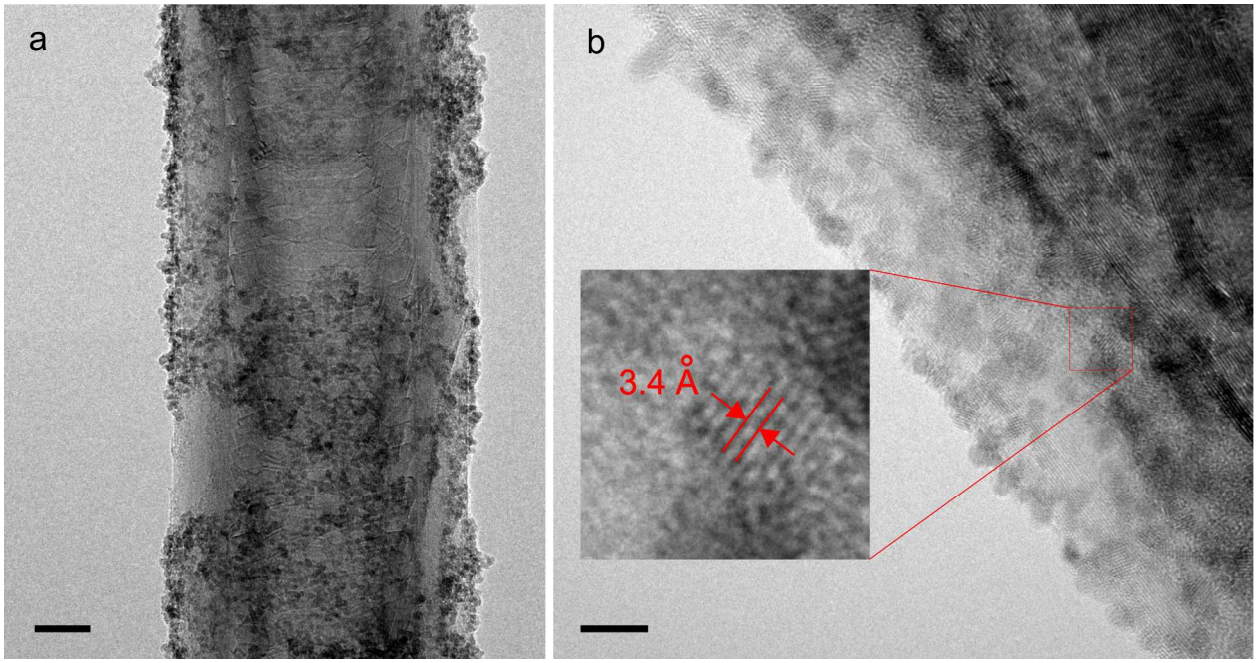

Figure 5. Representative TEM images of sensitized CNFs. a) Sensitized with 60 mM HCl. Large patches of tin free carbon are visible (scale bar, 20 nm). b) Sensitized with 160 mM HCl solution. The distribution of tin particles is uniform and amounts to roughly 1.5×10^5 particles/μm^2. The inset shows the crystal plane distance of 3.4 Å, which is consistent with SnO_2 (scale bar, 5 nm).

We performed XPS analysis on dried sensitized particles. Figure 6 shows the spectra of Sn 3d and O 1s peaks on the sensitized sample. As SnO and SnO_2 $3d_{5/2}$ peaks are very close together, the 3d peak by itself is not enough to confirm the oxidation state for Sn(IV). The usual way to proceed in this case is to assess the value of the Auger parameter which is unaffected by surface charge. It is defined as the sum of the kinetic energy of the Sn $M_4N_{45}N_{45}$ peak with the binding energy of the Sn $3d_{5/2}$ peak. In our case, the Auger energy is found at 431.7 eV for an Auger parameter value of 919.2 eV. This indicates that tin is tetravalent in the dried samples. Moreover, the stoichiometry shows a 2.1 at. % ratio between the tin SnO_X and the oxygen Sn-O binding

energies, indicating 2 oxygen atoms for every SnO_X detected. We can therefore more confidently state that all tin oxidizes to SnO_2 upon drying. This provides an explanation to the historically known fact that sensitized surfaces must not be allowed to dry before silver deposition [55].

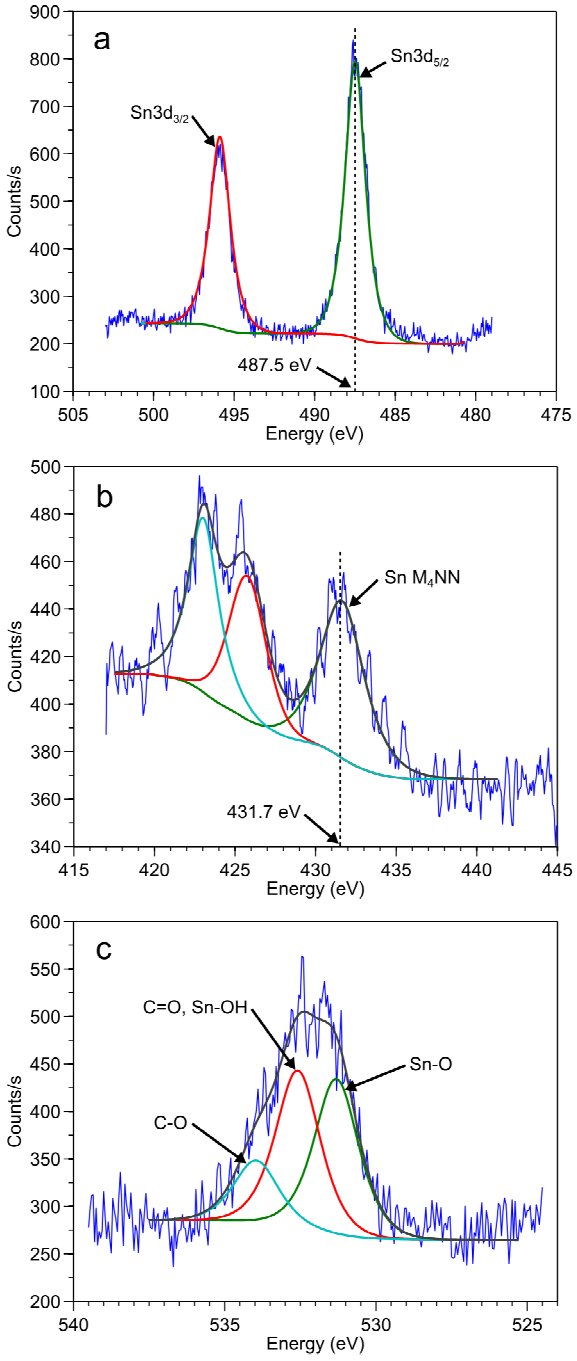

Figure 6. High resolution XPS spectra of tin-sensitized CNFs. a) Shows the tin peak with the usual 1.5 ratio between $Sn3d_{3/2}$ and $Sn3d_{5/2}$ peak areas. The $Sn3d_{5/2}$ peak is found at 487.5 eV. b) Sn Auger peaks. The kinetic energy of the Sn $M_4N_{45}N_{45}$ is found at 431.7 eV and adds to the $Sn3d_{5/2}$ energy for an Auger parameter of 919.2, which indicates that tin is under the Sn(IV)

oxidation state. c) Oxygen 1s peak. The Sn-O_X stoichiometry further confirms that tin is tetravalent.

3.2. SILVER DEPOSITION

Silver deposition is performed by electroless deposition through diamminesilver ions reduction by the dextrose aldehyde group. Deposition on small structures such as CNFs requires control over the silver particles growth rate. The literature conveys many examples relating a smooth and uniform deposition to a slower deposition rate [24, 56-57]. However, Boehm *et al*. showed that an optimal surface plasmon resonance signal, which the authors correlate with a good surface smoothness, coincided with the maximum deposition rate, keeping all variables constant except potassium hydroxide content in the diamminesilver solution [26]. They nevertheless found that increasing the plating rate by increasing the temperature was detrimental to the film quality. All aldehydes can reduce silver in the Tollens' scheme. Using dextrose as a reducing agent yielded a lower deposition rate and better results than formaldehyde in terms of coating uniformity and density. We therefore proceeded to investigate dextrose-reduced reactions. The silver solution was prepared fresh for every experiment following the 1:500 [KOH]:[Ag] ratio found optimal for surface plasmon resonance on microscope slides by Boehm *et al.* [26].

We first proceeded to investigate the effect of the amount of Tollens' reagent in solution. Silver solution was added to the samples in increasing volumes. The dispersions were then filtered and extensively rinsed with deionized water, resulting in layers of nanoparticles evenly spread on polycarbonate filter membranes so that sheet conductivity measurements are possible. Since all samples have the same area and starting amount of carbon material, sheet conductivity and mass data points are directly comparable. These values are plotted in Figure 7-a. The mass of

samples increases linearly with the Ag solution amount. As the total sample mass is in all cases well under the mass of silver in solution, the increasing number of silver ions cannot solely explain the change of mass between samples. Another explanation lies in the increasing deposition rate because of the reaction media getting more alkaline as more ammonia and KOH is added [58]. The sheet conductivity data has more complex behavior. For a Ag/KOH molar ratio below 0.7, the conductivity increases very slightly, but jumps suddenly by more than one order of magnitude as the molar ratio reaches 0.8. As the weight of samples increases in a nearly linear fashion, the conductivity is not proportional to the samples' weight. This is further confirmed in Figure 7-b, where the specific conductivity (sheet conductivity per unit area density) is plotted. Considering a uniform layer of metal, one would expect the specific conductivity to remain constant as more silver is added. However, a sudden increase is observed here as well.

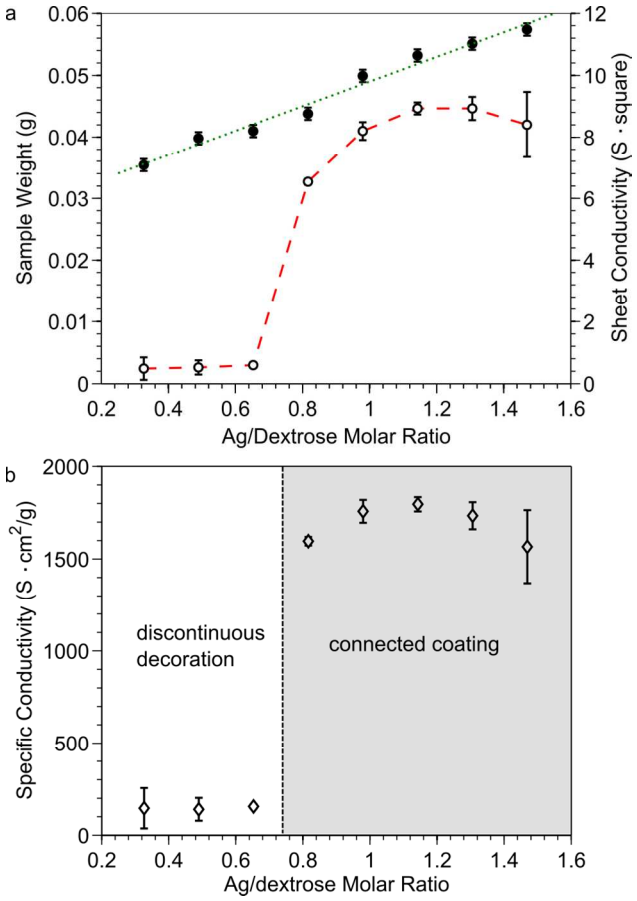

Figure 7. Electrical properties of hybrid nanoparticles as a function of silver to dextrose molar ratio. a) A linear trend appears in sample mass (●) while the electrical conductivity (o) undergoes a sudden change at 0.8 molar ratio. b) Specific conductivity (◊) of the samples. The sudden increase in conductivity is even more apparent here.

The behavior is explained by the morphology of the silver deposits on the different samples. Figure 8 shows SEM images of samples with 0.65, 0.81, 1.14 and 1.47 Ag/dextrose molar ratios, corresponding to the samples before and after the sudden jump in conductivity, at maximum specific conductivity and at highest silver solution volume. The silver deposits for 0.65 molar ratio (Figure 8 a and b) exhibit a disconnected morphology with large patches of bare carbon. In

this situation, the silver network on the connected 2-d geometry of the carbon particles' surface is not achieved. Therefore, the conduction properties are in large part attributable to the carbon transport properties. Figure 8-b shows a magnified view of a large silver cluster. These clusters can be found all over the sample. They are detrimental to the specific conductivity as they do not participate in the network but add a considerable amount of mass to the sample. In strong contrast, at 0.81 molar ratio (Figure 8 c and d) silver shows preferential formation on the surface of the nanofibers and no large aggregates are found. Although some carbon is visible through the coating, a fully connected network of silver is deposited on the surface. The sample at 1.14 molar ratio (Figure 8 e and f) also shows a fully connected morphology without large aggregates. In this case, however, the visible patches of carbon are fewer, which favors the electrical conductivity by limiting the bottlenecks created by coating inhomogeneities. At 1.47 molar ratio (Figure 8-g and h), the sample shows a connected network of silver, but also exhibits the large aggregates discussed before. Overall the coating is not as homogeneous as in the 1.14 molar ratio sample, which means that the mass is used less effectively in transporting charges. Keeping all other parameters constant, only values of 0.8 to 1.5 Ag/dextrose molar ratios will yield coated rather than decorated particles, with an optimal value between 1.0 and 1.3 mL.

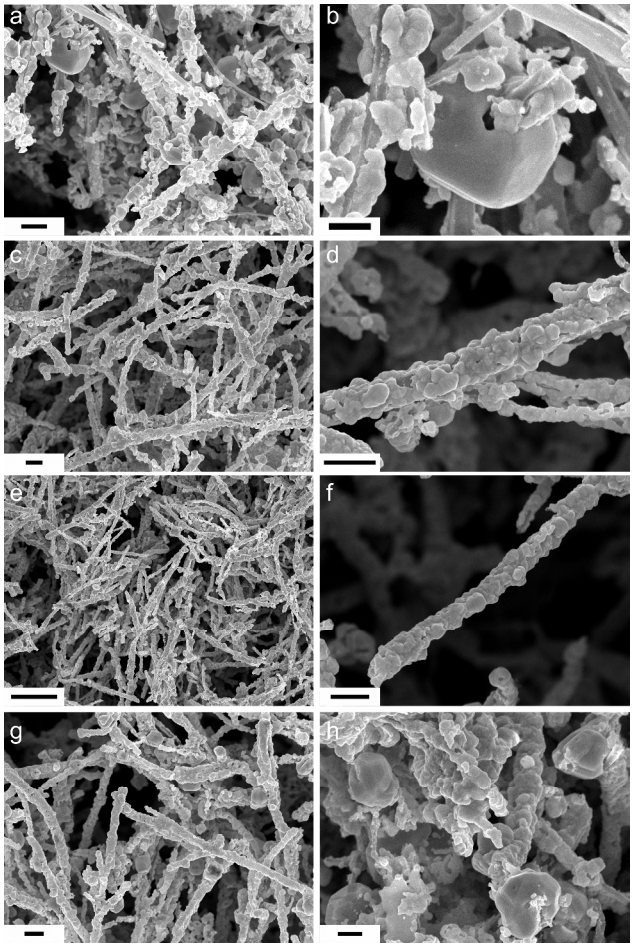

Figure 8. SEM images of samples with different Tollens' reagent contents. a) bulk view of sample at molar ratio 0.65. The coating is disconnected and large isolated silver aggregates are visible (scale bar 1 μm). b) close-up of a large silver crystal at 0.65 molar ratio (scale bar 500 nm). c) Bulk view of sample at molar ratio 0.81. The coating morphology suddenly transitioned from disconnected to mostly connected and uniform. No large aggregates are visible (scale bar 1 μm). d) Close-up of the silver coating at 0.81 molar ratio. Silver deposits are connected but some bare patches are visible (scale bar 1 μm). e) Bulk view of sample at 1.14 molar ratio corresponding to the maximum specific conductivity. All fibers are coated evenly and no large aggregates are visible (scale bar 5 μm). f) Close-up view of sample at 1.14 molar ratio. No bare carbon patches are visible (scale bar 1 μm). g)-h) Sample at 1.47 molar ratio. The coating is

uniform and no bare patches are visible, but large aggregates are visible (scale bars 1 μm and 500 nm, respectively). The coating becomes continuous somewhere around 0.8 molar ratio.

We then proceeded to investigate the concentration of reducing agent in solution. The reaction was performed with 3.5 mL Tollens' reagent, corresponding to the maximum specific conductivity in Figure 7 (molar ratio 1.14). Filtration and measurements were performed as for the prior investigation. Figure 9 shows the variation of weight, conductivity and specific conductivity of the hybrid nanoparticles filtered films. What first stands out is that the samples mass increases at first but starts to decrease after reaching the dextrose/Ag molar ratio of 4. The initial increase in mass can be explained by that the fact that dextrose is the limiting factor in this region, hence not all silver is allowed to react. Indeed, the sample mass reaches a plateau after dextrose and silver reach stoichiometric equilibrium (molar ratio dextrose/Ag of 0.5).

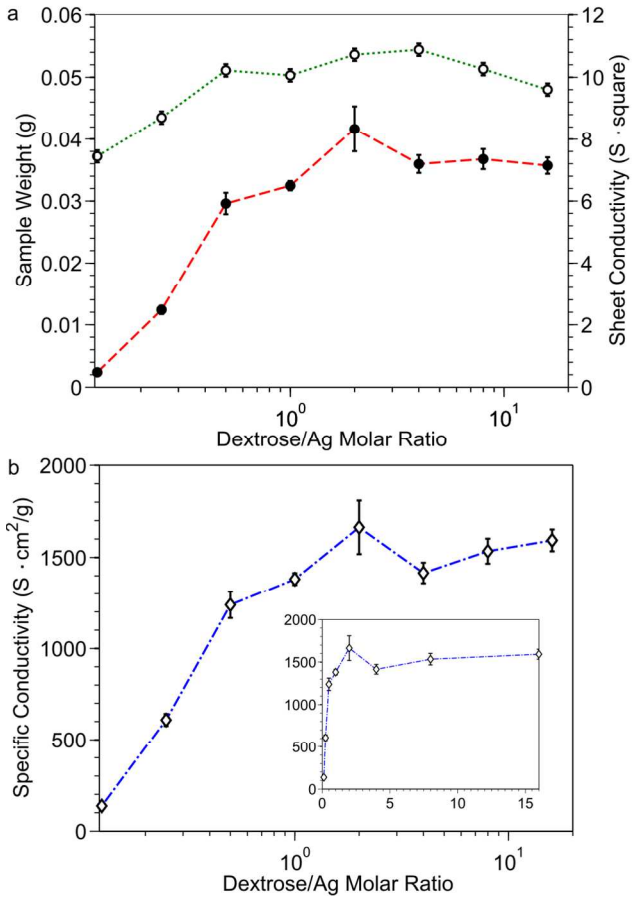

Figure 9. Electrical properties with respect to Dextrose to silver molar ratio. a) Mass (●)and sheet conductivity (○). The mass of samples stays fairly constant over the 0.5 molar ratio, consistant with a stoichiometric concentration of dextrose. As dextrose is in excess, the sample mass stays constant. b) Specific conductivity (◊). The values remain mostly constant for glucose in excess. The inset provides the same values on a linear scale for comparison with Figure 7.

Figure 10 shows SEM images of samples with various dextrose concentrations. The image on the left is an overview of each sample's appearance while the image on the right provides a close-up on the coating morphology. At 0.25 molar ratio (Figure 10-a and b), the metallic silver does not form a uniform layer, but rather deposits in large 100-500 nm islands. Large micron-

sized aggregates are also visible which are not present at higher dextrose concentration. This suggests that dextrose as a limiting factor does not simply stop the reaction before a uniform coating is obtained but produces a less controlled reaction resulting in larger crystals and poor coverage. Differences between molar ratios 1 (Figure 10-c and d) and 4 (Figure 10-e and f) are not significant, with a slightly more uniform coating with more dextrose. Figure 9-a shows that the sample mass decreases slightly after a molar ratio of 4, which could be attributable to a slower reaction rate because of a reduced diffusion owing to a higher viscosity. The slight decrease in sample mass is not mirrored by a decrease in conductivity, and no clear trend is observed in the specific conductivity (Figure 9-b) for a molar ratio above unity. While adding Tollens' reagent in excess destabilizes the reaction, both Figure 9 and Figure 10 suggest that adding dextrose up to 32 times the stoichiometric amount is not detrimental to the reaction. The deposition behavior is thus far more sensitive to the amount of Tollens' reagent than it is to dextrose concentration. Furthermore, it was noticed that a high dextrose concentration helped to prevent the aggregation of particles during the electroless deposition process. It is therefore recommended that dextrose be used well in excess of the stoichiometric dextrose/Ag ratio of 0.5.

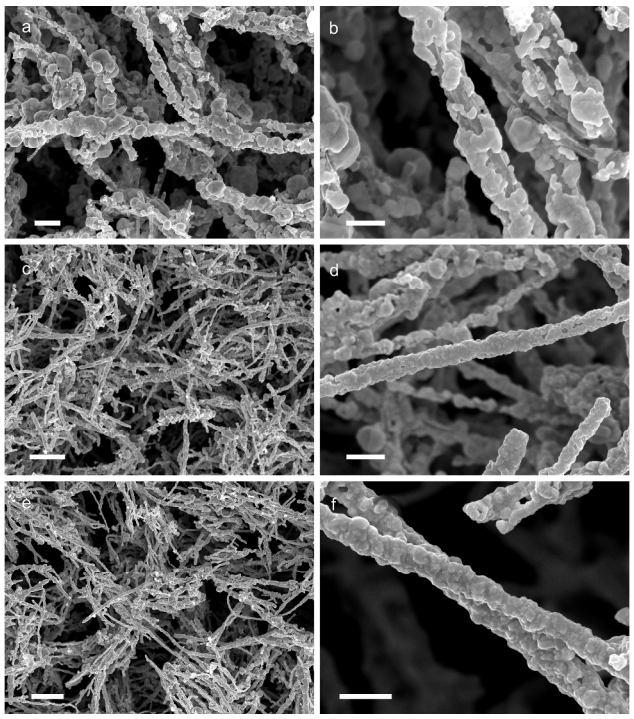

Figure 10. SEM images of samples with different dextrose concentrations. a) and b) Sample #2. Silver metal forms in disconnected 100-500 nm thick islands. Scale bars are a) 1 μm and b) 500 nm. c) Bulk view of sample #4. All fibers are coated and the silver is connected. Scale bar is 5 μm. d) close-up view of a fiber from sample 4. Some bare patches of carbon are visible. Scale bar is 1 μm. e) and f) Sample #6. All fibers are uniformly coated. No bare patches are visible. Scale bars are e) 5μm and f) 1 μm.

The highest specific conductivity we measured on a 10 cm^2 bulk hybrid silver-CNFs sample was 1800 $S \cdot cm^2/g$ which is only roughly one order of magnitude lower than the specific conductivity of pure silver. The thickness of this film was of 127 μm for a density of 0.4 g/cm^3 (supporting information, Figure S1), which suggests that an efficient conduction network is achieved at only 4% volume loading since the particles' density can be approximated to that of silver. This finding is of crucial importance, since the loading required for percolation in

conductive adhesives is around 20-30%. This exceptionally low volume loading can be explained by the high aspect ratio of the particles which allows for a much more efficient conductivity network. It is thought that the particles undergo oxidation upon drying as some samples went from a yellow to a grey tint. This might explain the difference between the maximum conductivities reached during the investigations of Tollens' reagent amount vs. dextrose amount in solution, as the samples from the latter exhibit a much darker tint (supporting information, Figure S2). It is however unclear why one series of experiment did undergo more oxidation than the other. We believe that it is linked to the rinsing procedure as the samples displayed less oxidation on the periphery of filtered cake. This part of the sample resides under the ridge of the clamped funnel and as such is subject to less water flow during the rinsing step (supporting information, Figure S3). This behavior suggests that protecting the particles with a capping agent such as poly(acrylic acid) might be an easy way to increase the conductivity of the material. As the process is easily scalable to arbitrarily large batches, the technology could replace the silver particles traditionally found in applications such as conductive inks and adhesives. The added value of the technology in this situation is two-fold: cost reduction as less silver metal is required to achieve an excellent conductivity and overall weight reduction which resonates with applications in the aerospace sector.

4. CONCLUSION

We provided a detailed analysis of all the main steps of the electroless silver deposition on CNFs, from the characterization of the starting material through functionalization and tin sensitization until silver deposition itself. We demonstrated that acid functionalization at temperatures lower than 45 °C could efficiently attach carboxylic groups on CNFs without

affecting their aspect ratio. We provided new insight into the tin sensitization process that supports a previously published theory on the matter and proposed an optimal HCl concentration for the sensitizing bath. We then provided a range of parameters for which the electroless deposition of silver reliably results in a smooth, continuous and uniform coating on high aspect ratio CNFs. The particles can be used as-produced without the need for time-consuming purification and can be recovered by simple vacuum filtration, thus eliminating the multiple centrifugation steps that plague silver nanowires fabrication processes. The process is scalable with no noted effect of the vessel size on any step of the process and no heat or damageable shear is required. The resulting bulk particles proved to be efficient in transporting current with a specific electrical conductivity of 1.8×10^3 $S \cdot cm^2/g$, roughly one order of magnitude lower than that of pure silver (6×10^4 $S \cdot cm^2/g$). The high aspect ratio allows for a more efficient conductivity network, since more contacts are allowed par particle and each particle can transport charges further. Moreover, the packing density of the nanoparticles is of the order of 4%, which indicates that not only are the particles more efficient than packed spherical nanoparticles, but they achieve a robust conduction network at a much lower volume fill ratio, as fillers used in adhesives reach percolation around 20-30 vol%. As such, the hybrid nanofibers are excellent candidates for conductive composites formulation as they offer both a lower weight and a lower cost of silver metal than typical silver flakes. Conductive adhesives and composites for lightning strike protection might therefore benefit from this technology. Since the particles maintain their high aspect ratio, they also exhibit a large surface area and might spark interest as high surface area electrodes. We aimed at providing a study of the deposition process as a whole. Some of its aspects remain unclear, such as the sensitizing dynamics, or the fundamental reasons for the unevenness of the silver deposition under certain conditions. Along with clarification on this

subject, optimization work on the pre-treatment steps could be undertaken to alleviate the time required for the manipulations. As our focus was on optimizing the deposition uniformity and the electrical conductivity of the particles, little work was consecrated to the time-wise efficiency of the process, and we believe that dramatic improvements could be achieved. As the technique might be valuable for metallizing a wide array of complex-shaped nanostructures in addition to the carbon nanofibers reported herein, many applications could benefit from additional research on the topic.

SUPPORTING INFORMATION

Information about the chemical reactions involved in electroless deposition. Measurement of a nanoparticles layer for assessment of particles packing and volume conductivity. Discussion about the oxidation of nanoparticles with associated photographs. This material is available free of charge via the Internet at http://pubs.acs.org.

AUTHOR INFORMATION

Corresponding Author

*Prof. Daniel Therriault

Département de Mécanique Appliquée

École Polytechnique de Montréal.

2900 Boul. Édouard-Montpetit

Montréal, Québec, Canada

H3T 1J4

Present Addresses

†If an author's address is different than the one given in the affiliation line, this information may be included here.

Author Contributions

The manuscript was written through contributions of all authors. All authors have given approval to the final version of the manuscript. ‡These authors contributed equally. (match statement to author names with a symbol)

Funding Sources

Conseil de Recherches en Sciences Naturelles et en Génie du Canada (CRSNG)

Fonds de Recherche du Québec – Nature et Technologie (FRQNT)

Bombardier Aerospace.

3M Corporation.

Bell Helicopter Textron.

ACKNOWLEDGMENTS

This work has been sponsored by the Consortium de Recherche et d'Innovation en Aérospatiale du Québec (CRIAQ project COMP-502) with financial contribution from industrial partners Bombardier Aerospace, Bell Helicopter Textron and 3M. Financial support for M. Cauchy was provided by the Fonds de Recherche du Québec – Nature et Technologie (FRQNT). The authors

also wish to acknowledge the gracious help of Josianne Lefebvre (GCM, École Polytechnique de Montréal) in acquiring and interpreting the XPS spectra.

REFERENCES

(1) Li, Y.; Wong, C. P., Recent Advances of Conductive Adhesives as a Lead-Free Alternative in Electronic Packaging: Materials, Processing, Reliability and Applications. Mater. Sci. Eng., R 2006**,** 51 (1-3), 1-35.

(2) Gagné, M.; Therriault, D., Lightning Strike Protection of Composites. Prog. Aerosp. Sci 2014**,** 64, 1-16.

(3) Veedu, V. P.; Cao, A.; Li, X.; Ma, K.; Soldano, C.; Kar, S.; Ajayan, P. M.; Ghasemi-Nejhad, M. N., Multifunctional Composites Using Reinforced Laminae with Carbon-Nanotube Forests. Nat. Mater. 2006**,** 5 (6), 457-462.

(4) Li, J.; Ma, P. C.; Chow, W. S.; To, C. K.; Tang, B. Z.; Kim, J. K., Correlations between Percolation Threshold, Dispersion State, and Aspect Ratio of Carbon Nanotubes. Adv. Funct. Mater. 2007**,** 17 (16), 3207-3215.

(5) Bao, W. S.; Meguid, S. A.; Zhu, Z. H.; Weng, G. J., Tunneling Resistance and Its Effect on the Electrical Conductivity of Carbon Nanotube Nanocomposites. J. Appl. Phys. 2012**,** 111 (9), 093726-093727.

(6) Bauhofer, W.; Kovacs, J. Z., A Review and Analysis of Electrical Percolation in Carbon Nanotube Polymer Composites. Compos. Sci. Technol. 2009**,** 69 (10), 1486-1498.

(7) Martin, C. A.; Sandler, J. K. W.; Shaffer, M. S. P.; Schwarz, M. K.; Bauhofer, W.; Schulte, K.; Windle, A. H., Formation of Percolating Networks in Multi-Wall Carbon-Nanotube–Epoxy Composites. Compos. Sci. Technol. 2004**,** 64 (15), 2309-2316.

(8) Ebbesen, T. W.; Lezec, H. J.; Hiura, H.; Bennett, J. W.; Ghaemi, H. F.; Thio, T., Electrical Conductivity of Individual Carbon Nanotubes. Nature 1996**,** 382 (6586), 54-56.

(9) Maiti, S.; Suin, S.; Shrivastava, N. K.; Khatua, B. B., A Strategy to Achieve High Electromagnetic Interference Shielding and Ultra Low Percolation in Multiwall Carbon Nanotube–Polycarbonate Composites through Selective Localization of Carbon Nanotubes. RSC adv 2014**,** 4 (16), 7979-7990.

(10) Shastry, T. A.; Seo, J. W.; Lopez, J. J.; Arnold, H. N.; Kelter, J. Z.; Sangwan, V. K.; Lauhon, L. J.; Marks, T. J.; Hersam, M. C., Large-Area, Electronically Monodisperse, Aligned Single-Walled Carbon Nanotube Thin Films Fabricated by Evaporation-Driven Self-Assembly. Small 2013**,** 9 (1), 45-51.

(11) Du, F.; Fischer, J.; Winey, K., Effect of Nanotube Alignment on Percolation Conductivity in Carbon Nanotube/Polymer Composites. Phys. Rev. B 2005**,** 72 (12).

(12) Buldum, A.; Lu, J. P., Contact Resistance between Carbon Nanotubes. Phys. Rev. B 2001**,** 63 (16).

(13) Ma, P. C.; Siddiqui, N. A.; Marom, G.; Kim, J. K., Dispersion and Functionalization of Carbon Nanotubes for Polymer-Based Nanocomposites: A Review. Compos Part a-Appl S 2010**,** 41 (10), 1345-1367.

(14) Hu, A.; Guo, J. Y.; Alarifi, H.; Patane, G.; Zhou, Y.; Compagnini, G.; Xu, C. X., Low Temperature Sintering of Ag Nanoparticles for Flexible Electronics Packaging. Appl. Phys. Lett. 2010**,** 97 (15), 153117.

(15) Perelaer, J.; Klokkenburg, M.; Hendriks, C. E.; Schubert, U. S., Microwave Flash Sintering of Inkjet-Printed Silver Tracks on Polymer Substrates. Adv. Mater. 2009**,** 21 (47), 4830-4834.

(16) Magdassi, S.; Grouchko, M.; Berezin, O.; Kamyshny, A., Triggering the Sintering of Silver Nanoparticles at Room Temperature. ACS Nano 2010**,** 4 (4), 1943-1948.

(17) Garnett, E. C.; Cai, W.; Cha, J. J.; Mahmood, F.; Connor, S. T.; Greyson Christoforo, M.; Cui, Y.; McGehee, M. D.; Brongersma, M. L., Self-Limited Plasmonic Welding of Silver Nanowire Junctions. Nat. Mater. 2012**,** 11 (3), 241-249.

(18) Wu, H. P.; Liu, J. F.; Wu, X. J.; Ge, M. Y.; Wang, Y. W.; Zhang, G. Q.; Jiang, J. Z., High Conductivity of Isotropic Conductive Adhesives Filled with Silver Nanowires. Int. J. Adhes. Adhes. 2006**,** 26 (8), 617-621.

(19) Tang, X.; Tsuji, M.; Jiang, P.; Nishio, M.; Jang, S.-M.; Yoon, S.-H., Rapid and High-Yield Synthesis of Silver Nanowires Using Air-Assisted Polyol Method with Chloride Ions. Colloids Surf. Physicochem. Eng. Aspects 2009**,** 338 (1-3), 33-39.

(20) Li, B.; Ye, S.; Stewart, I. E.; Alvarez, S.; Wiley, B. J., Synthesis and Purification of Silver Nanowires to Make Conducting Films with a Transmittance of 99%. Nano Lett. 2015**,** 15 (10), 6722-6726.

(21) Zhang, P.; Wyman, I.; Hu, J.; Lin, S.; Zhong, Z.; Tu, Y.; Huang, Z.; Wei, Y., Silver Nanowires: Synthesis Technologies, Growth Mechanism and Multifunctional Applications. Mater. Sci. Eng., B 2017**,** 223, 1-23.

(22) Wadsworth, F. L. O., Notes on Silvering Solutions and Silvering. Astrophys. J 1895**,** 1, 252-260.

(23) Curtis, H. D., Methods of Silvering Mirrors. Publ. Astron. Soc. Pac 1911**,** 23, 13-32.

(24) Malureanu, R.; Zalkovskij, M.; Andryieuski, A.; Lavrinenko, A. V., Controlled Ag Electroless Deposition in Bulk Structures with Complex Three-Dimensional Profiles. Journal of The Electrochemical Society 2010**,** 157 (12), K284.

(25) Formanek, F.; Takeyasu, N.; Tanaka, T.; Chiyoda, K.; Ishikawa, A.; Kawata, S., Selective Electroless Plating to Fabricate Complex Three-Dimensional Metallic Micro/Nanostructures. Appl. Phys. Lett. 2006**,** 88 (8), 083110.

(26) Boehm, J.; François, A.; Ebendorff-Heidepriem, H.; Monro, T. M., Chemical Deposition of Silver for the Fabrication of Surface Plasmon Microstructured Optical Fibre Sensors. Plasmonics 2010**,** 6 (1), 133-136.

(27) Cheng, M. L.; Tsai, B. C.; Yang, J., Silver Nanoparticle-Treated Filter Paper as a Highly Sensitive Surface-Enhanced Raman Scattering (Sers) Substrate for Detection of Tyrosine in Aqueous Solution. Anal. Chim. Acta 2011**,** 708 (1-2), 89-96.

(28) Park, H. K.; Lee, H. B.; Kim, K., A Facile Deposition of Silver onto the Inner Surface of a Glass Capillary Tube for Micro-Surface-Enhanced Raman Scattering Measurements. Appl. Spectrosc. 2007**,** 61 (1), 19-24.

(29) Tongxiang, L.; Wenli, G.; Yinghui, Y.; Chunhe, T., Electroless Plating of Silver on Graphite Powders and the Study of Its Conductive Adhesive. Int. J. Adhes. Adhes. 2008**,** 28 (1-2), 55-58.

(30) Chueh, T. C.; Hu, C. H.; Yen, S. C., Electrically Conductive Adhesives with Low Ag Content Prepared by Ag Self-Activated Plating and Pedot:Pss. J. Electrochem. Soc. 2015**,** 162 (1), D56-D61.

(31) Zheng, J.-w.; Wang, Z.-l.; Qiao, L.; Cai, W.; Jiang, L.-q.; Ying, Y.; Che, S.-l., Fabrication of Ag–C Composite Materials with Core–Shell Structure. Appl. Surf. Sci. 2014**,** 313, 346-351.

(32) Shukla, S.; Seal, S.; Rahaman, Z.; Scammon, K., Electroless Copper Coating of Cenospheres Using Silver Nitrate Activator. Mater. Lett. 2002**,** 57 (1), 151-156.

(33) Chakravarthi, D. K.; Khabashesku, V. N.; Vaidyanathan, R.; Blaine, J.; Yarlagadda, S.; Roseman, D.; Zeng, Q.; Barrera, E. V., Carbon Fiber-Bismaleimide Composites Filled with Nickel-Coated Single-Walled Carbon Nanotubes for Lightning-Strike Protection. Adv. Funct. Mater. 2011**,** 21 (13), 2527-2533.

(34) Lin, Y.; Watson, K. A.; Fallbach, M. J.; Ghose, S.; Smith, J. G., Jr.; Delozier, D. M.; Cao, W.; Crooks, R. E.; Connell, J. W., Rapid, Solventless, Bulk Preparation of Metal Nanoparticle-Decorated Carbon Nanotubes. ACS Nano 2009**,** 3 (4), 871-884.

(35) Wang, F.; Arai, S.; Endo, M., Metallization of Multi-Walled Carbon Nanotubes with Copper by an Electroless Deposition Process. Electrochem. Commun. 2004**,** 6 (10), 1042-1044.

(36) Wang, Y.; Xu, X.; Tian, Z.; Zong, Y.; Cheng, H.; Lin, C., Selective Heterogeneous Nucleation and Growth of Size-Controlled Metal Nanoparticles on Carbon Nanotubes in Solution. Chemistry 2006**,** 12 (9), 2542-2549.

(37) Ang, L. M.; Hor, T. S. A.; Xu, G. Q.; Tung, C. H.; Zhao, S. P.; Wang, J. L. S., Decoration of Activated Carbon Nanotubes with Copper and Nickel. Carbon 2000**,** 38 (3), 363-372.

(38) Córdoba, J. M.; Odén, M., Growth and Characterization of Electroless Deposited Cu Films on Carbon Nanofibers. Surf. Coat. Technol. 2009**,** 203 (22), 3459-3464.

(39) Silvain, J. F.; Richard, P.; Douin, J.; Lahaye, M.; Heintz, J. M., Electroless Coating Process of Carbon Nano Fibers by Copper Metal. Mater. Sci. Forum 2007**,** 534-536, 1445-1448.

(40) Tamayo-Ariztondo, J.; Córdoba, J. M.; Odén, M.; Molina-Aldareguia, J. M.; Elizalde, M. R., Effect of Heat Treatment of Carbon Nanofibres on Electroless Copper Deposition. Compos. Sci. Technol. 2010**,** 70 (16), 2269-2275.

(41) Arai, S.; Imoto, Y.; Suzuki, Y.; Endo, M., Fabrication of Ni–B Alloy Coated Vapor-Grown Carbon Nanofibers by Electroless Deposition. Carbon 2011**,** 49 (4), 1484-1490.

(42) Arai, S.; Kobayashi, M.; Yamamoto, T.; Endo, M., Pure-Nickel-Coated Multiwalled Carbon Nanotubes Prepared by Electroless Deposition. Electrochem. Solid-State Lett. 2010**,** 13 (12), D94.

(43) Arai, S.; Fujii, J., Electroless Deposition of Silver on Multiwalled Carbon Nanotubes Using Iodide Bath. J. Electrochem. Soc. 2011**,** 158 (8), D506.

(44) Hung, N. T.; Tuong, N. M.; Rakov, E. G., Acid Functionalization of Carbon Nanofibers. Inorg. Mater. 2010**,** 46 (10), 1077-1083.

(45) Ros, T. G.; van Dillen, A. J.; Geus, J. W.; Koningsberger, D. C., Surface Oxidation of Carbon Nanofibres. Chem. Eur. J 2002**,** 8 (5), 1151-1162.

(46) Przyłuski, J.; Kasprzak, M.; Bieliński, J., Investigations of Sncl2-Sensitizing Solutions for Electroless Plating. Surf. Coat. Technol. 1987**,** 31 (3), 203-211.

(47) Wei, X.; Roper, D. K., Tin Sensitization for Electroless Plating Review. J. Electrochem. Soc. 2014**,** 161 (5), D235-D242.

(48) Tharwat, F. T., *Dispersion of Powders in Liquids and Stabilization of Suspensions*. Wiley-VCH: Hoboken, NJ, USA, **2012**.

(49) D'Amico, J. F.; De Angelo, M. A.; Henrickson, J. F.; Kenney, J. T.; Sharp, D. J., Selective Electroless Metal Deposition Using Patterned Photo-Oxidation of Sn(Ii) Sensitized Substrates. J. Electrochem. Soc. 1971**,** 118 (10), 1695-1699.

(50) Cohen, R. L.; West, K. W., Solution Chemistry and Colloid Formation in the Tin Chloride Sensitizing Process. J. Electrochem. Soc. 1972**,** 119 (4), 433-438.

(51) Cohen, R. L.; D'Amico, J. F.; West, K. W., MöSsbauer Study of Tin(Ii) Sensitizer Deposits on Kapton. J. Electrochem. Soc. 1971**,** 118 (12), 2042-2046.

(52) Feldstein, N.; Weiner, J. A.; Schnable, G. L., Some Aspects of the Chemistry of Tin Sensitizing Solutions. J. Electrochem. Soc. 1972**,** 119 (11), 1486-1490.

(53) Batzill, M.; Diebold, U., The Surface and Materials Science of Tin Oxide. Prog. Surf. Sci. 2005**,** 79 (2-4), 47-154.

(54) Su, D.; Ahn, H. J.; Wang, G., Sno2@Graphene Nanocomposites as Anode Materials for Na-Ion Batteries with Superior Electrochemical Performance. Chem Commun (Camb) 2013**,** 49 (30), 3131-3133.

(55) King, E. S., Silvering Mirrors, with Plate Ix. Popular Astronomy 1922, 93-95.

(56) Antonello, A.; Jia, B.; He, Z.; Buso, D.; Perotto, G.; Brigo, L.; Brusatin, G.; Guglielmi, M.; Gu, M.; Martucci, A., Optimized Electroless Silver Coating for Optical and Plasmonic Applications. Plasmonics 2012**,** 7 (4), 633-639.

(57) Feng, Y.; Yuan, H., Electroless Plating of Carbon Nanotubes with Silver. Journal of Materials Science 2004**,** 39 (9), 3241-3243.

(58) Schlesinger, M.; Paunovic, M., Modern Electroplating. Wiley, c., Ed. Hoboken, NJ, **2010**.

TOC graphics: